Final Report
NCC3-719

CENTRIFUGAL COMPRESSOR AEROELASTIC ANALYSIS CODE

submitted to

National Aeronautics and Space Administration
Glenn Research Center at Lewis Field
Cleveland, Ohio

Dr. Theo G. Keith, Jr.
Distinguished University Professor

Dr. Rakesh Srivastava
Senior Research Associate

Department of Mechanical Industrial and Manufacturing Engineering
The University of Toledo
Toledo, Ohio 43606

CENTRIFUGAL COMPRESSOR AEROELASTIC ANALYSIS CODE

Introduction

Centrifugal compressors are very widely used in the turbomachine industry where low mass flow rates are required. Gas turbine engines for tanks, rotorcraft and small jets rely extensively on centrifugal compressors for rugged and compact design. These compressors experience problems related with unsteadiness of flowfields, such as stall flutter, separation at the trailing edge over diffuser guide vanes, tip vortex unsteadiness, etc., leading to rotating stall and surge. Considerable interest exists in small gas turbine engine manufacturers to understand and eventually eliminate the problems related to centrifugal compressors. The geometric complexity of centrifugal compressor blades and the twisting of the blade passages makes the linear methods inapplicable. Advanced computational fluid dynamics (CFD) methods are needed for accurate unsteady aerodynamic and aeroelastic analysis of centrifugal compressors. Most of the current day industrial turbomachines and small aircraft engines are designed with a centrifugal compressor. With such a large customer base and NASA Glenn Research Center being the lead center for turbomachines, it is important that adequate emphasis be placed on this area as well. Currently, this activity is not supported under any project at NASA Glenn.

Centrifugal compressors experience essentially the same problems associated with unsteadiness as axial compressors. Separated flows lead to a significant drop in performance. Problems associated with stall flutter lead to blade loss that further deteriorates the performance. Because of the complex shape, a CFD based aerodynamic solver is needed to accurately calculate the unsteady airloads. Further, since the primary instability is either stall flutter or surge, the aeroelastic solver requires viscous analysis capabilities.

A viscous aeroelastic or unsteady aerodynamic analysis capability will help design safer, lighter and more reliable engines. Because of a more accurate estimate of the unsteady aerodynamic forces improved blades can be designed that will help move instability boundaries away from the engine operating range. The increased safety margin will allow operation at higher efficiencies resulting in lower fuel consumption and reduction in exhaust gas pollutants such as CO_2, NOx

and hydrocarbons. A better blade design will reduce or eliminate the flutter and forced response problems resulting in lower maintenance costs and less risk of blade failure.

Currently there are no viscous aeroelastic analysis codes for centrifugal compressor geometries available to industry users. Industry, especially the small engine manufacturers, are extremely interested in obtaing the capability of unsteady aerodynamic and aeroelastic analyses of centrifugal compressor. Under the cooperative agreement with NASA (NCC3-719), development of a tool based on a viscous aerodynamic analysis code, TURBO [1], was undertaken to address this short coming and provide industry users with a robust aeroelastic analysis code for centrifugal compressors. Cuts in funding by almost 50 percent for the last two years of the project and unforeseen additional code modifications, restricted us from completely accomplishing the final objective. However, significant progress was made in developing an unsteady aerodynamic solver applicable to impeller geometry. The TURBO-AE code [2], an aeroelastic analysis code for axial turbomachinery geometry, based on the TURBO code, was successfully modified for analysis of centrifugal impellers with and without splitters. The code was validated by applying it to a Low Speed Centrifugal Compressor (LSCC) geometry. Results showed good agreement with measured data. Also, the modifications made to the code were furnished to researchers at Mississippi State University (MSU), the developers of the TURBO code, to incorporate the modifications into later versions of the code.

Accomplishments

The goal of this effort was to suitably modify and extend the capabilities of the TURBO-AE aeroelastic code for application to centrifugal compressors. The TURBO-AE code is a viscous aeroelastic program for axial turbomachinery components. It has been developed with funding from the AST program. Further development of the TURBO-AE code is continuing with funding from the Ultra Efficient Engine Technology (UEET) and the Quiet Aircraft Technology (QAT) programs. The modified TURBO-AE code was applied to the LSCC geometry for validating the code modifications.

The TURBO and the TURBO-AE codes have been developed for axial flow turbomachinery configurations and as such possess several inherent assumptions that would not allow a solution of a centrifugal geometry. The codes, for example, assume the flow to be predominantly in the axial direction with the in-flow and out-flow boundaries being nearly perpendicular to the flight direction. This assumption is used to simplify the inlet and exit boundary conditions. Also, the

orientation of the boundary plane is used in defining the deformations to simulate the blade vibrations. This dependence on the orientation of the exit plane had to be modified to make the code compatible with centrifugal compressor geometry. Further, the interpolations of mode shapes from structural to aerodynamic grids assume the blades to be more or less planar. This is not the case for centrifugal compressors, which require a more sophisticated interpolation program. Also, since the basic grid layouts are significantly different from the axial flow geometry, dynamic grid deformation routines - used to simulate blade flexibility, had to be modified as well.

During the course of this project, several other problems were encountered associated with coding issues. For example, the code did not have the capability of using multiple blocks per blade passage. This became an issue with larger grids. Further, the coding did not permit leading or trailing edges to have different indices for different blades. This prohibited the analysis of impellers with splitter blades. Both of these issues required significant code modifications that were not anticipated at the beginning of the work. Because of reductions in funding, all of the required modifications could not be completed. However, in the following, tasks that were accomplished during the project will be described.

Code Modifications

The following major modifications were made to the TURBO-AE code to allow for the analysis of a centrifugal impeller.

Flow Initialization: TURBO code initializes the flowfield based on the starting condition for the flow condition. If a flow solution is available, it is used to initialize the flowfield for further analysis. In the absence of an existing solution, the flowfield is initialized with uniform far field conditions. For axial flow configuration the flow through the turbomachine is primarily axial, however, for the centrifugal machines the flow turns by 90 deg with the exit flow being discharged with a significant radial velocity component. Initializing the flow with uniform axial flowfield caused numerical problems in starting the analysis. This required modification of flow initialization for the centrifugal impeller geometry. The modifications were made by initializing the flow conditions to be parallel to the hub and casing and normal to blade passage at each flow location, keeping the total flow conditions the same as the farfield conditions. The passage normal was determined by taking the area normal of the plane formed at the constant i-plane. However, no account was made for the pressure rise due to radial displacement because of change of radial location in the flow path.

Splitter Geometry: Significant effort was required to adapt the coding to handle a splitter blade. Most CFD codes inherently assume the *i*-indices for leading and trailing edges for all blades to be same for a blade row. This built-in assumption within the TURBO-AE code had to be modified in order to enable the analysis of geometries with splitter blades. Further, the TURBO-AE code solves the flowfield of one blade passage with the blade surfaces located at the two ends of the passage. This meant that the leading and trailing edge indices for the two surfaces across the same passage needed to differ from one another. This flexibility of indices has implications on the application of the surface or fluid passage boundary condition since the indices define the solid surfaces of the blades. This required modifying significant portions of the code to allow for blade passage and surface dependent solid surface definition and indices.

Another significant modification dictated by the need for handling splitter geometry was the fact that the grid for one blade passage would be too large and thereby poses a problem with computer resources. Consequently, the original passage had to be split into at least two passages. The TURBO code assumed that a single blade passage constituted a single analysis block. This required modifying the code to allow for the analysis of multiple blocks per blade passage. Significant effort was required in making modifications to the code to permit this change. The modifications were restricted to two blocks per blade passage to keep the modifications to a minimum. More blocks per passage would have required modifying the boundary layer application routines resulting in significantly more code modifications. Multiple blocks per passage required modifications to boundary condition applications, performance calculations, distance to wall calculation for viscous analysis, and so forth.

Exit Boundary: The most significant modifications were required for the implementation of exit boundary conditions. The TURBO code applies characteristics boundary conditions at the exit plane in Cartesian coordinates. The exit grid plane is assumed to be normal to the x-axis to simplify the boundary conditions. For a radial machine, neither the exit plane is normal to x-axis, nor is it Cartesian. This required the development of characteristic boundary conditions in radial coordinates simplified by the assumption of the exit plane grid being in the radial plane.

For subsonic exit flow boundary conditions, four characteristics are extrapolated from inside the flow domain with the fifth characteristic being fixed at the boundary. For a supersonic exit boundary, all five characteristics are extrapolated from inside the domain. The characteristics at the boundary are obtained as follows

$$\left(\frac{W_k}{J}\right)_b^{n+1} = \left(\frac{W_k}{J}\right)_b^{n} + \nabla\tau\left[\left(\frac{\bar{s}}{J}\right)_b - \Lambda_k \frac{\left(\frac{W_k}{J}\right)_{i+\frac{1}{2}}^{n} - \left(\frac{W_k}{J}\right)_{i-\frac{1}{2}}^{n}}{\Delta k}\right] \tag{1}$$

where, W_k is the characteristic, J is the Jacobian, $\nabla\tau$ is the time step, Λ_k is the eigenvalue, n is the iteration counter, and subscript b refers to the boundary. For the five characteristics $\frac{W_k}{J}$ and $\frac{\bar{s}}{J}$ are defined as follows

$$\frac{W_k^1}{J} = \rho - \frac{p}{c_0^2} \quad \text{and} \quad \frac{\bar{s}_1}{J} = \frac{u_r}{r}\left(\frac{\gamma p}{c_0^2} - \rho\right)$$

$$\frac{W_k^2}{J} = u_x \quad \text{and} \quad \frac{\bar{s}_2}{J} = 0$$

$$\frac{W_k^3}{J} = -u_\theta \quad \text{and} \quad \frac{\bar{s}_3}{J} = \frac{u_r u_\theta}{r}$$

$$\frac{W_k^4}{J} = \frac{1}{\sqrt{2}}\left(\frac{p}{\rho_0 c_0} + u_r\right) \quad \text{and} \quad \frac{\bar{s}_4}{J} = \frac{1}{r\sqrt{2}}\left(u_\theta^2 - \frac{\gamma u_r p}{\rho_0 c_0}\right)$$

$$\frac{W_k^5}{J} = \frac{1}{\sqrt{2}}\left(\frac{p}{\rho_0 c_0} - u_r\right) \quad \text{and} \quad \frac{\bar{s}_5}{J} = -\frac{1}{r\sqrt{2}}\left(u_\theta^2 - \frac{\gamma u_r p}{\rho_0 c_0}\right)$$

where, u_x, u_r, and u_θ are velocity components in the axial, radial and tangential directions, respectively, ρ is the fluid density, p is the pressure, c is the speed of sound, r is the radius, and γ is the gas constant. The subscript 0 refers to reference quantities.

For a subsonic exit boundary condition application, the exit static pressure is fixed based on the pressure ratio of the operating condition and the first four characteristics are extrapolated to the boundary using Eq.(1). The characteristic values are converted to primitive variables using he definition provided above. For a supersonic exit boundary all five characteristics are extrapolated. The primitive variables obtained in cylindrical coordinates at the exit plane are then converted back to the Cartesian coordinates.

Post Processing: A significant effort was also devoted to developing post processing capabilities in order to compare the calculated results with measured data. Fluid velocity and blade surface pressure have been measured at various locations with measurement planes being normal to the mean flow direction. This required development of interpolation routines to transfer calculated flow properties from the aerodynamic grid onto the plane of measurement. Since the flow path is highly three-dimensional, special attention had to be paid to finding the correct set of points from which to interpolate. Further, the measured static surface pressure has been reduced to account for the centrifugal force exerted on the fluid. In order to compare the pressure with measured data, the following normalization was used based on the formulation described in Ref. [3]

$$\frac{p_r}{p_{std}} = \frac{p}{p_{std}} \left(\frac{h - \frac{1}{2}\omega^2 r^2}{h} \right)^{\frac{\gamma}{\gamma - 1}} \tag{2}$$

where, p_r is the reduced pressure, p_{std} is a reference pressure, p is the calculated pressure, h is enthalpy, ω is the rotational speed, and r is the radius.

The code modifications to TURBO were made in modular form without disturbing the original computational capabilities.

A grid generation program entitled TIGER [6] was also evaluated for use with grid generation of a centrifugal geometry. However, the program was found to be difficult and cumbersome to use for grid generation of LSCC. This program was abandoned in favor of a grid generation program available at NASA Glenn.

MSU researchers are currently involved in developing a parallel version of the TURBO code. The modifications made to the TURBO-AE code were forwarded to researchers at MSU to import the appropriate modifications into the parallel code. This will enable industry users to employ one code for various turbomachinery applications.

Code Validation

The modified code was tested and validated for aerodynamic analysis capability by applying the code to analyze the Low Speed Centrifugal Compressor (LSCC). This compressor impeller has been thoroughly tested in a NASA Glenn wind tunnel [4], and provides for an excellent test case to verify and validate the modified code for performance calculations.

The LSCC is an axial flow impeller with 20 blades, tip diameter of 1.524 m and a back sweep angle of 55 deg. The impeller was tested near its designed operating point with a mass flow of 30 kg/s and a rotational speed of 1,862 rpm. The test conditions were such that the flow was entirely subsonic through the impeller. The test was conducted using a vaneless diffuser that generated an axisymmetric outflow boundary condition, desirable for CFD analysis of an isolated blade row. The analysis using the modified TURBO-AE code was carried out using a grid with 129 grid points in the flow direction (m-direction), 61 grid points between the hub and the casing (span-direction), and 41 grid points in the blade-to-blade direction (tht-direction). Because of the size of the grid, the analysis was carried out using two grid blocks per blade passage in the blade-to-blade direction.

Figure 1 shows the impeller analyzed with pressure contours on its solid surfaces. The casing of the impeller is not shown for sake of clarity. Comparison of blade surface static pressure is shown in Figure 2. The pressure was normalized using Eq.(2) for comparison with experimental data. This normalization removes the pressure rise due to increase in the radius as the fluid travels from the leading edge to the trailing edge and provides the pressure variation because of blade passage diffusion. Very good agreement of the surface pressures with measured data was found. Also, shown on this figure is the comparison of performance characteristics of the impeller as compared with experimental measurements. Once again excellent agreement was obtained.

Figures 3 through 10 show comparisons of the velocity distributions. Comparisons are shown for the variation of the three velocity components (axial, radial, and tangential) normalized by the impeller tip speed at three span locations. The variation is shown for the blade passage at each streamwise location with suction surface being at 0 and pressure surface being at 100 on the horizontal axis. Flow velocity predictions were found to be in good agreement with measured values, however the comparisons of the velocities in the wake were found to possess only qualitative agreement. It is believed that the differences in the wake velocities were due to the use of the Baldwin-Lomax turbulence model in the code. This turbulence model does not accurately capture the characteristics of the blunt trailing edge of the blades. This resulted in the calculated flow leaving the surface at a slightly different angle than experimentally observed. Nevertheless, overall the agreement of the flow velocity was found to be good.

Concluding Remarks

A viscous analysis code applicable to centrifugal impeller geometry was developed and validated using experimental data. The code was developed by modifying the TURBO-AE code, which is applicable to axial flow turbomachinery components. The exit flow boundary conditions were developed and implemented in the TURBO-AE code along with several other modifications. Significant effort was expended to modify the code architecture to allow analysis with multiple blocks per blade passage and to allow for different i-indices for the leading and trailing edges of different blades. Predicted values manifested good agreement with measured data of surface pressure, performance quantities, and velocity components. However, the comparison of velocity distribution in the wake was found to be fair to poor, especially in the area near the casing. It was determined that the differences in the wake velocity predictions were primarily due to the inadequacy of the Baldwin-Lomax turbulence model. It is suggested that the k-ε turbulence model be added to the code to improve the velocity predictions. Also, further validation of a high-speed impeller geometry should be carried out.

References

1. Janus, J. M., "Advanced Three-Dimensional CFD Algorithm for Turbomachinery," Ph.D. Dissertation, Mississippi State University, May 1989.

2. Bakhle, M., Srivastava, R., Keith, T. Jr., Stefko, G. L., "A 3D Euler/Navier-Stokes Aeroelastic Code for Propulsion Applications," AIAA Paper 97-2749, 33rd Joint Propulsion Conference and Exhibit at Seattle, WA, July 1997.

3. Rautaheimo, P., Salminen, E., Siikonen, T., "Numerical Simulation of the Flow in the NASA Low-Speed Centrifugal Compressor", Report 119, Helsinki University of Technology, Helsinki, Finland.

4. Hathway, M. D., Chriss, R. M., Strazisar, A. J., and Wood, J. R., "Laser Anemometer Measurements of the Three-Dimensional Rotor Flow Field in the NASA Low-Speed Centrifugal Compressor.

5. Skoch, G. J., Prahst, P. S., Wernet, M. P., Wood, J. R., and Strazisar, A. J., "Laser Anemometer Measurements of the Flow Field in a 4:1 Pressure Ratio Centrifugal Impeller", NASA TM 107541, June 1997.

6. Shih, Ming-Hsin and Chen Yen-Sen, "TIGER Grid Generation Code," Final Technical Report for NASA Contract Number NAS-3-2775, ESI-TR-97-07, September 1997.

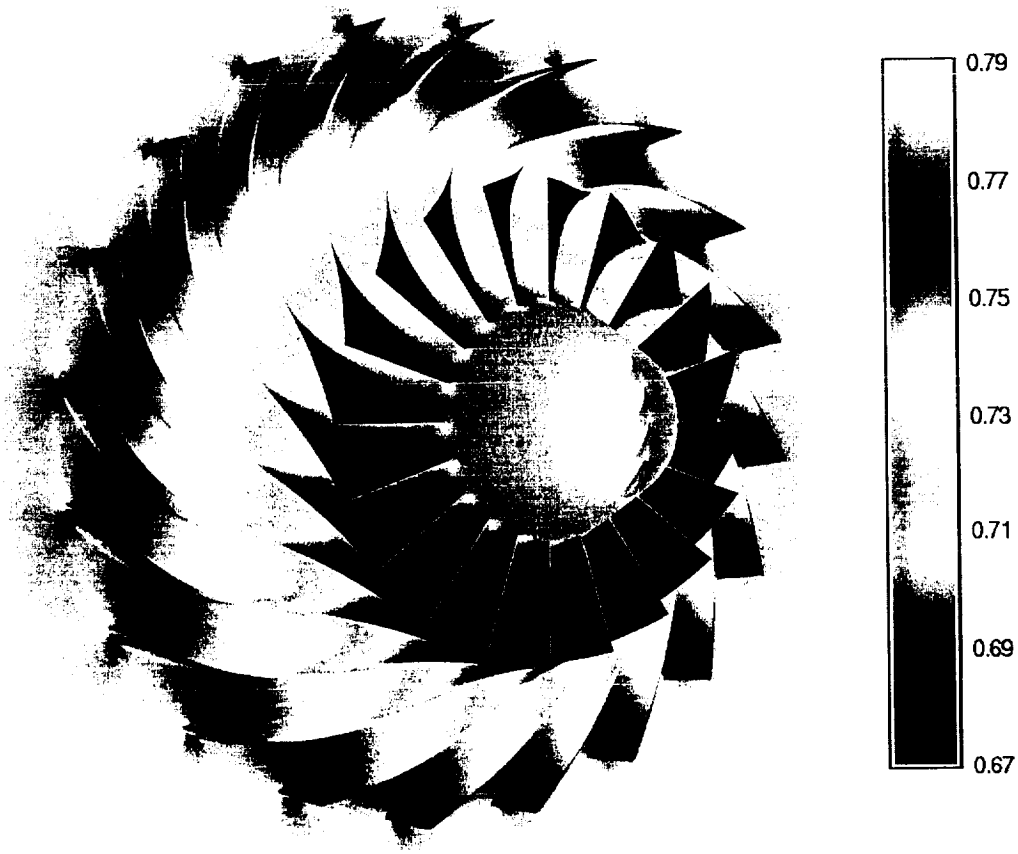

Figure 1. Steady pressure distribution on solid surfaces of the impeller

Calculated: Adiab. Eff.=0.916, Mass Avg. Temp Ratio=1.041, Energy Avg. Press. Ratio=1.138
Measured: Adiab. Eff.=0.922, Mass Avg. Temp Ratio=1.042, Energy Avg. Press. Ratio=1.141

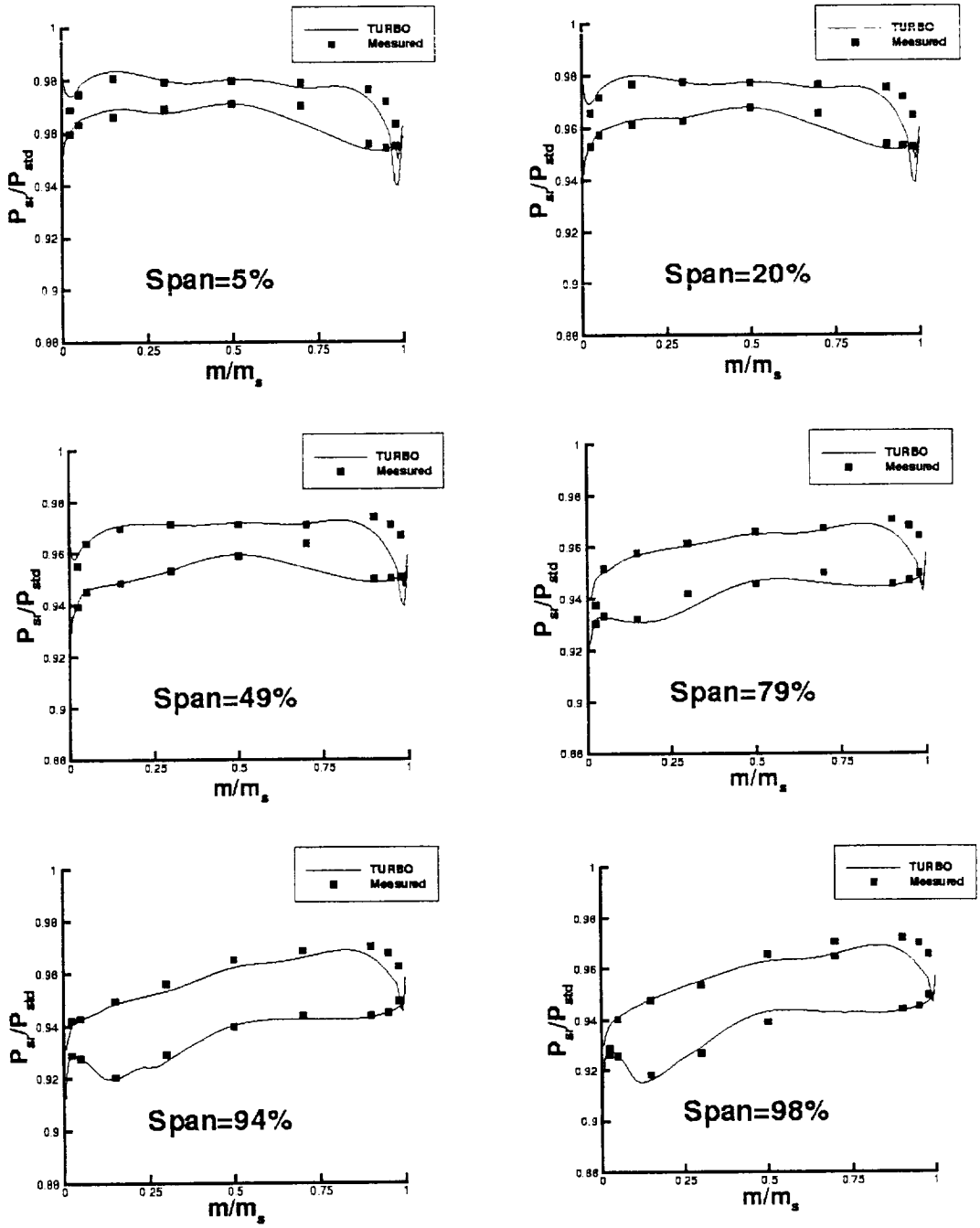

Figure 2. Comparison of blade surface static pressure for the LSCC at design condition at various span locations.

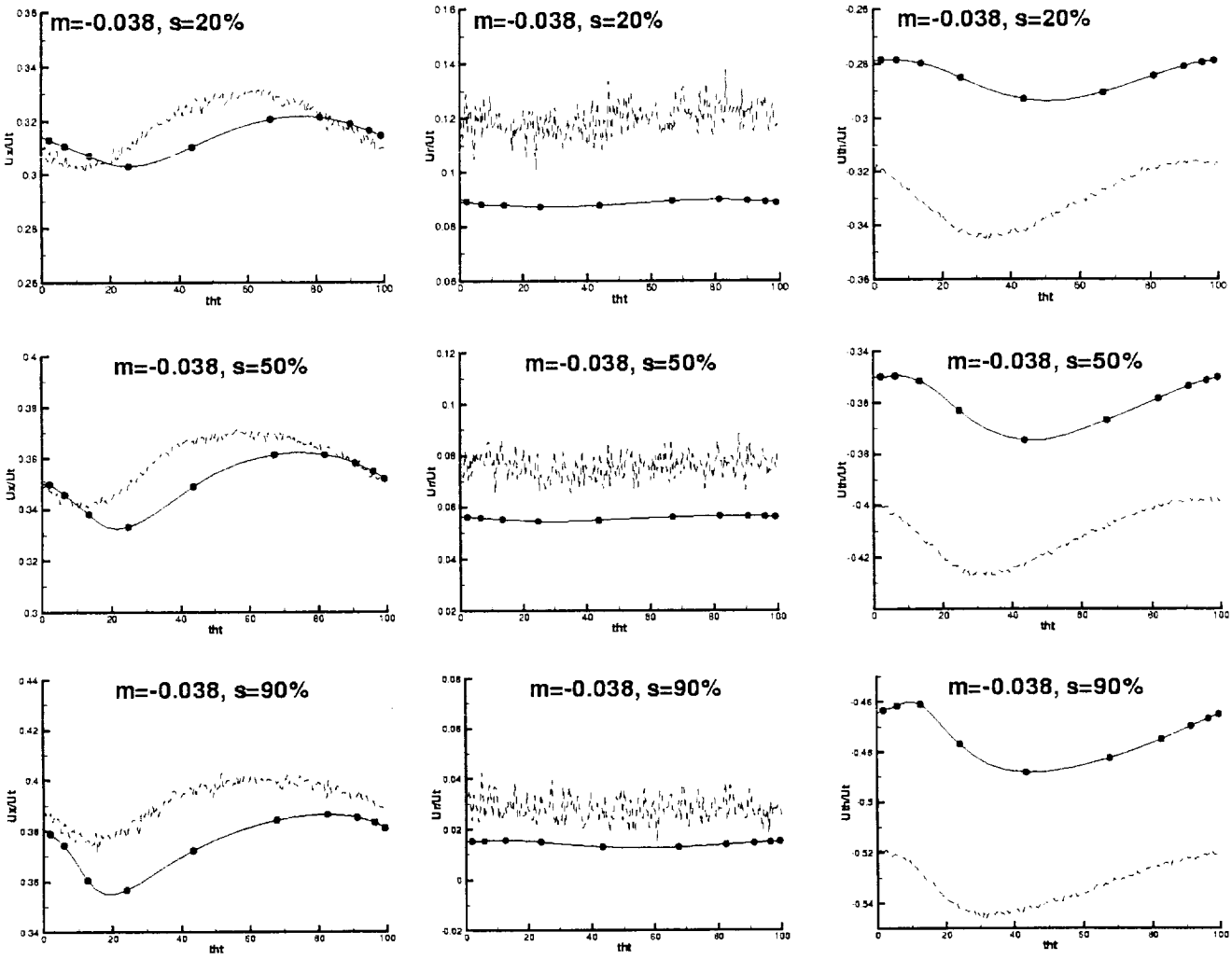

Figure 3. Comparison of axial, tangential and rotational velocity components in blade passage at 3.8 percent of chord length upstream of the blade at 20, 50 and 90 percent span stations. ---- Measured velocities, —— predicted TURBO predicted velocities.

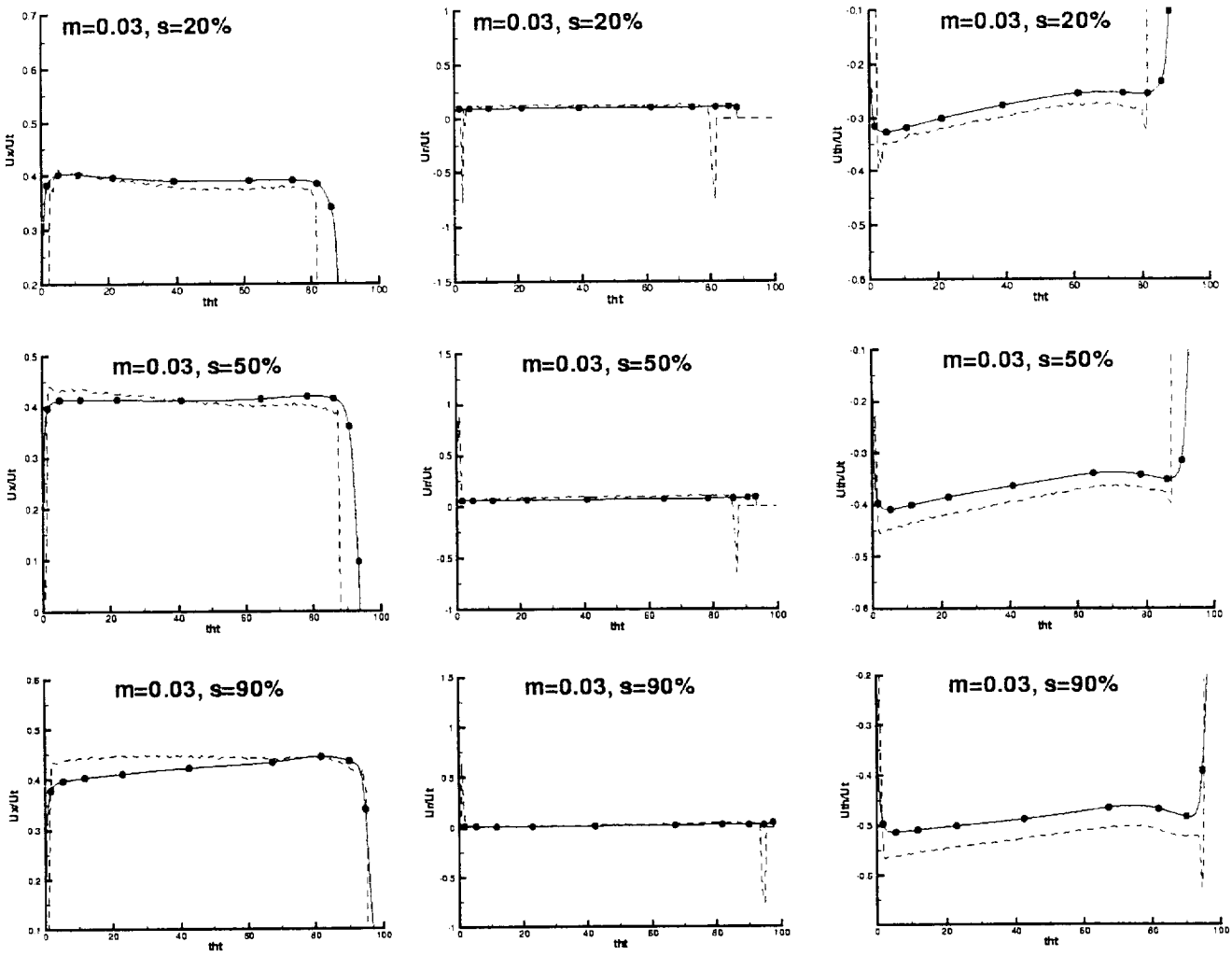

Figure 4. Comparison of axial, tangential and rotational velocity components in blade passage at 3.8 percent of chord length downstream of leading edge of the blade at 20, 50 and 90 percent span stations. ---- Measured velocities, —— predicted TURBO predicted velocities.

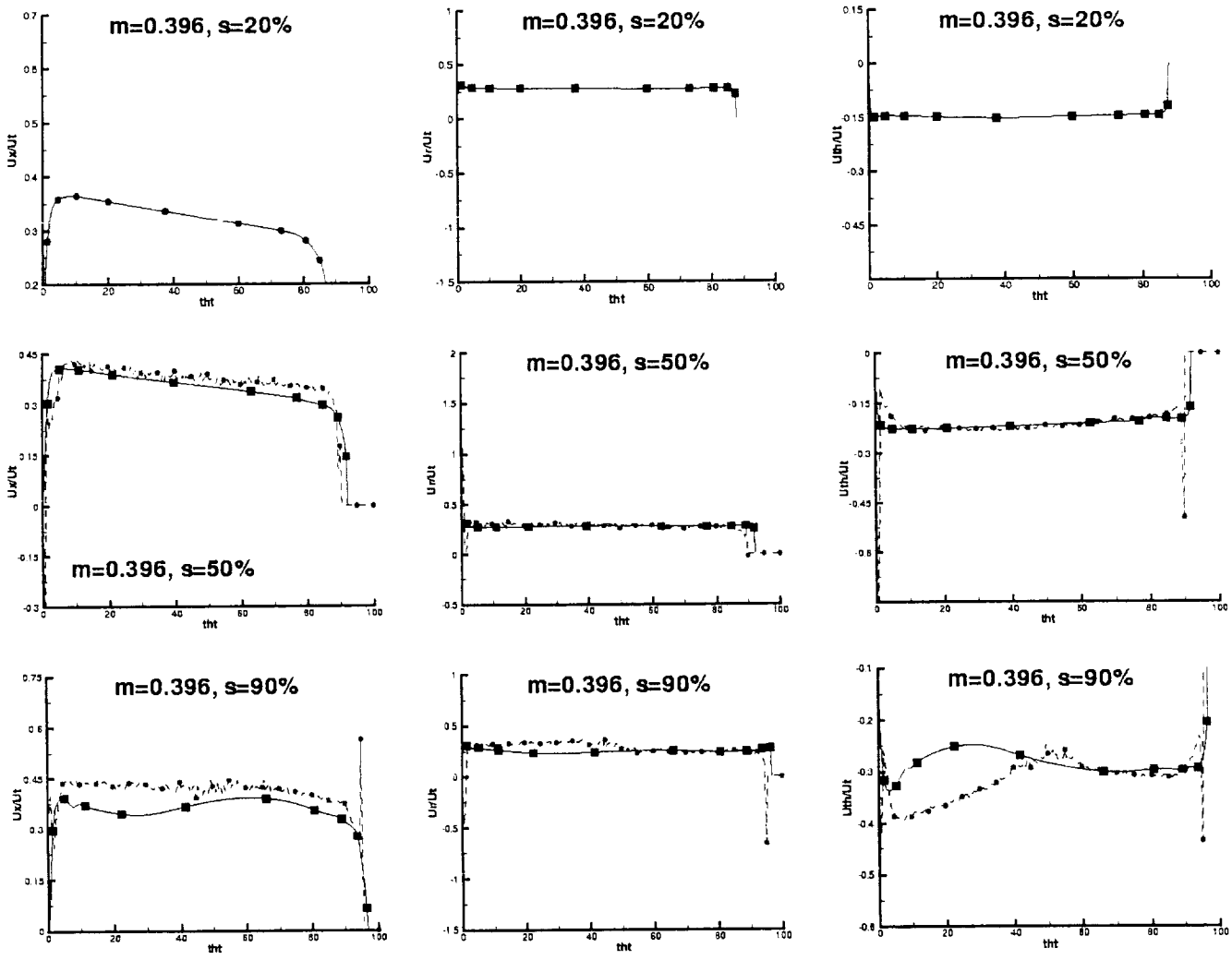

Figure 5. Comparison of axial, tangential and rotational velocity components in blade passage at 39.6 percent of chord length downstream of blade leading edge 20, 50 and 90 percent span stations. ---- Measured velocities, —— predicted TURBO predicted velocities.

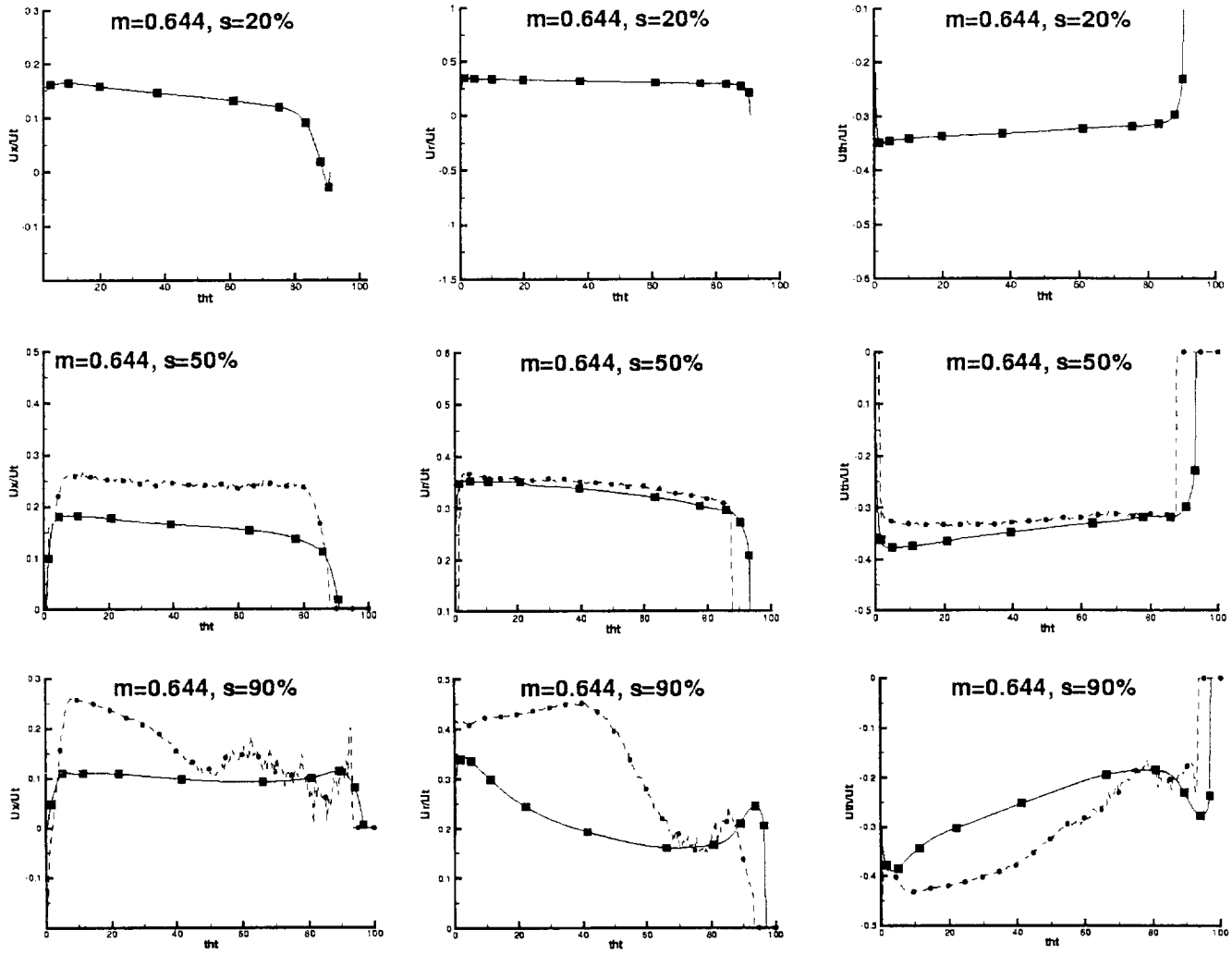

Figure 6. Comparison of axial, tangential and rotational velocity components in blade passage at 64.4 percent of chord length downstream of blade leading edge at 20, 50 and 90 percent span stations. ---- Measured velocities, —— predicted TURBO predicted velocities.

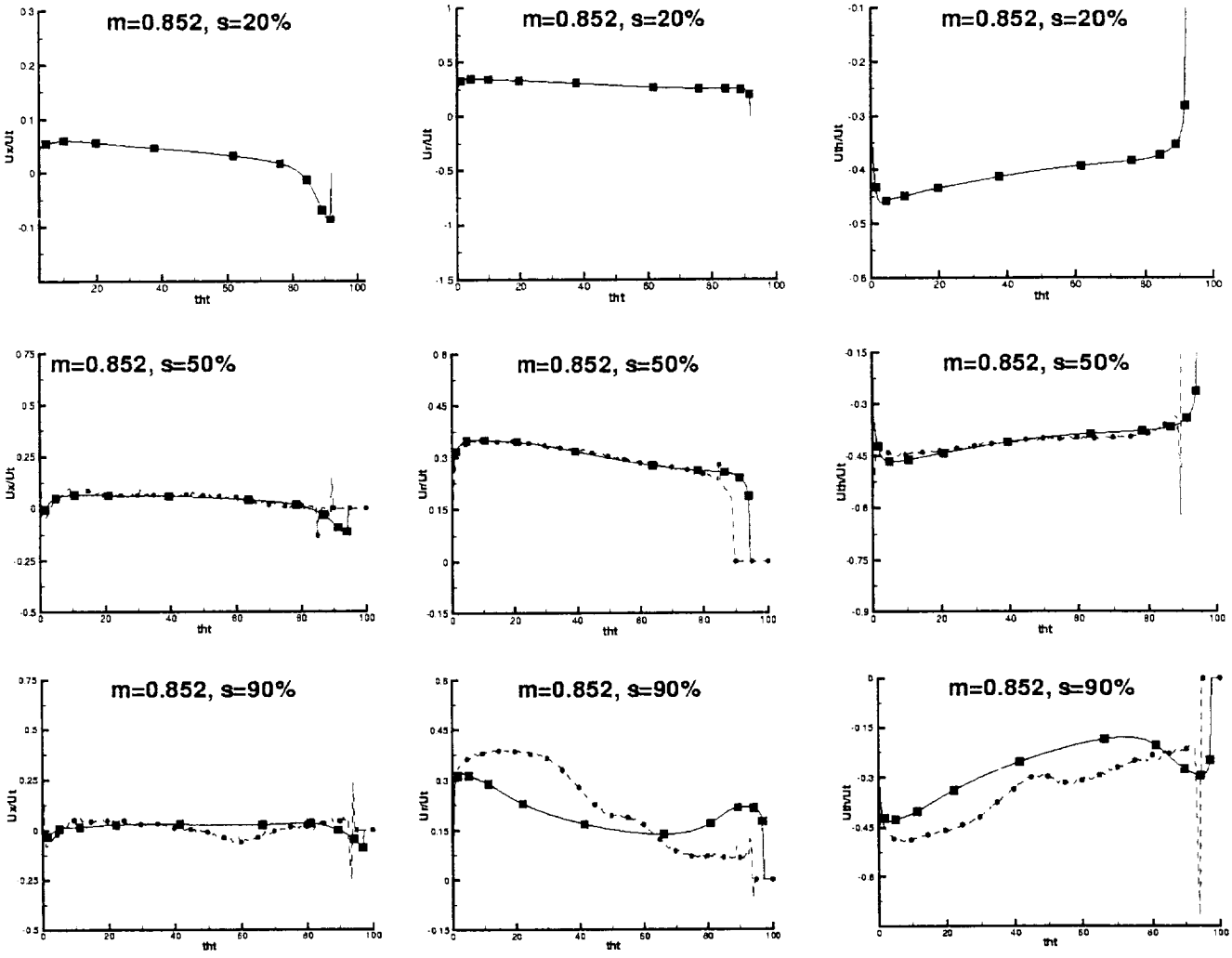

Figure 7. Comparison of axial, tangential and rotational velocity components in blade passage at 85.2 percent of chord length downstream of blade leading edge at 20, 50 and 90 percent span stations. ---- Measured velocities, —— predicted TURBO predicted velocities.

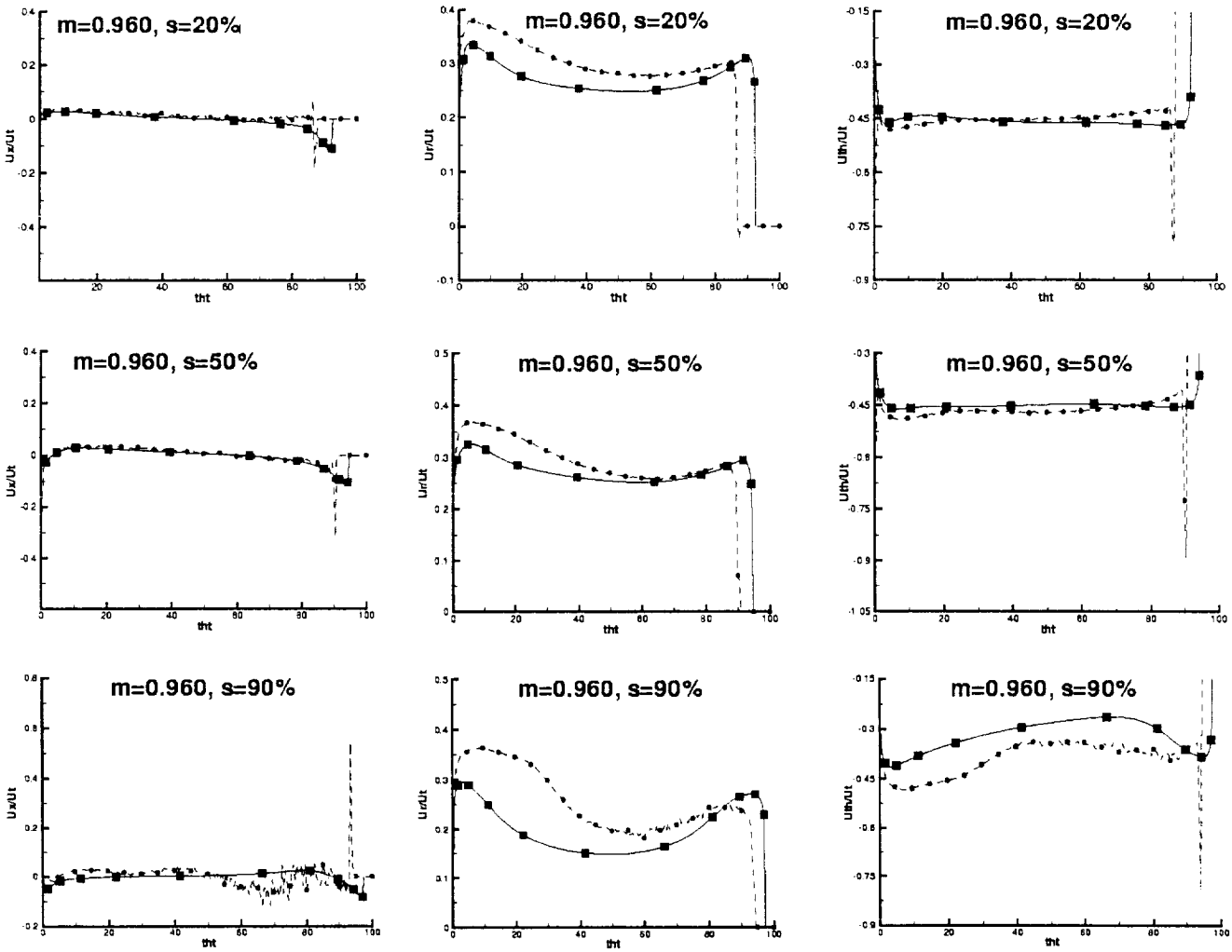

Figure 8. Comparison of axial, tangential and rotational velocity components in blade passage at 96 percent of chord length downstream of blade leading edge at 20, 50 and 90 percent span stations. ---- Measured velocities, —— predicted TURBO predicted velocities.

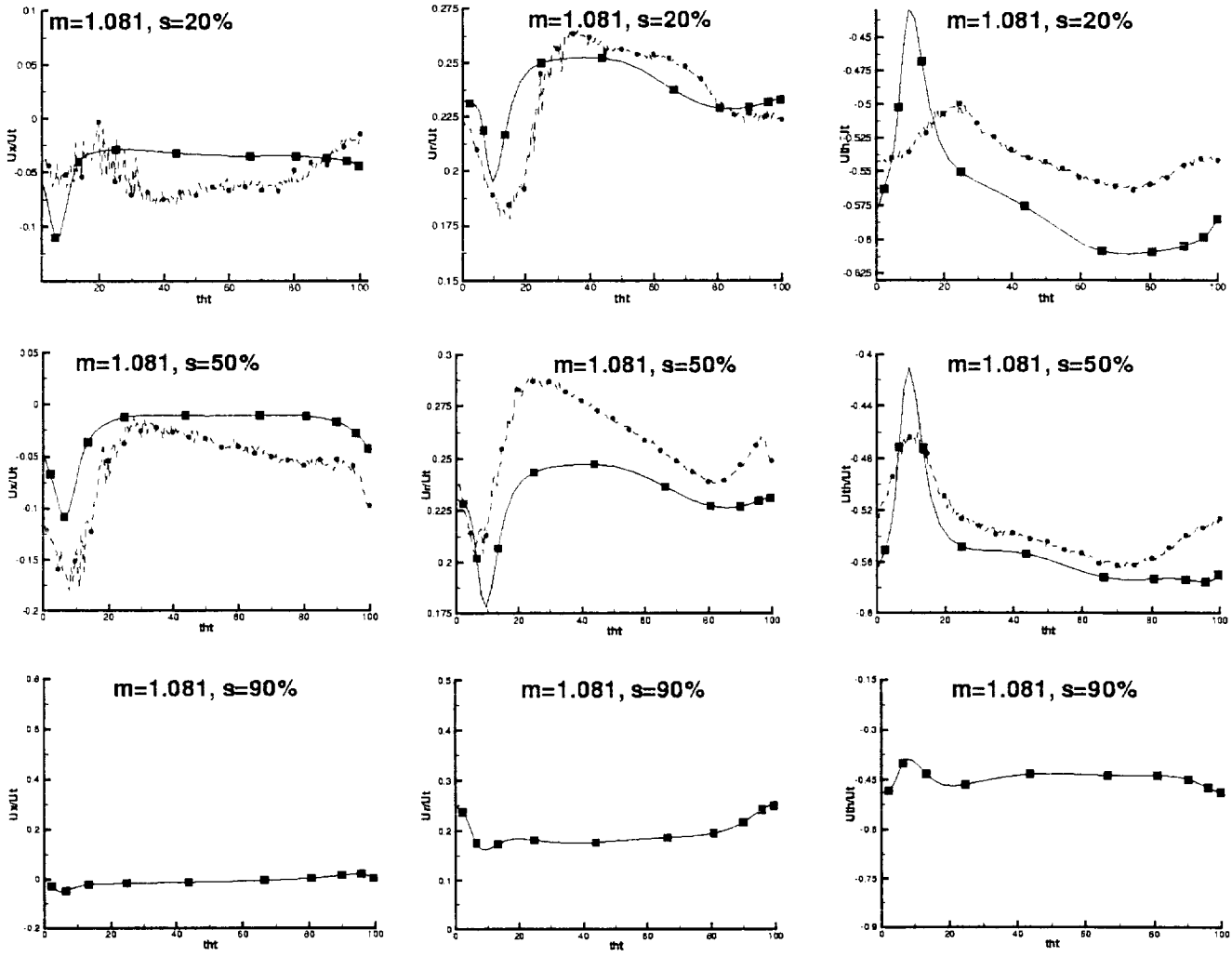

Figure 9. Comparison of axial, tangential and rotational velocity components in blade passage at 8.1 percent of chord length downstream of blade trailing edge at 20, 50 and 90 percent span stations. ---- Measured velocities, —— predicted TURBO predicted velocities.

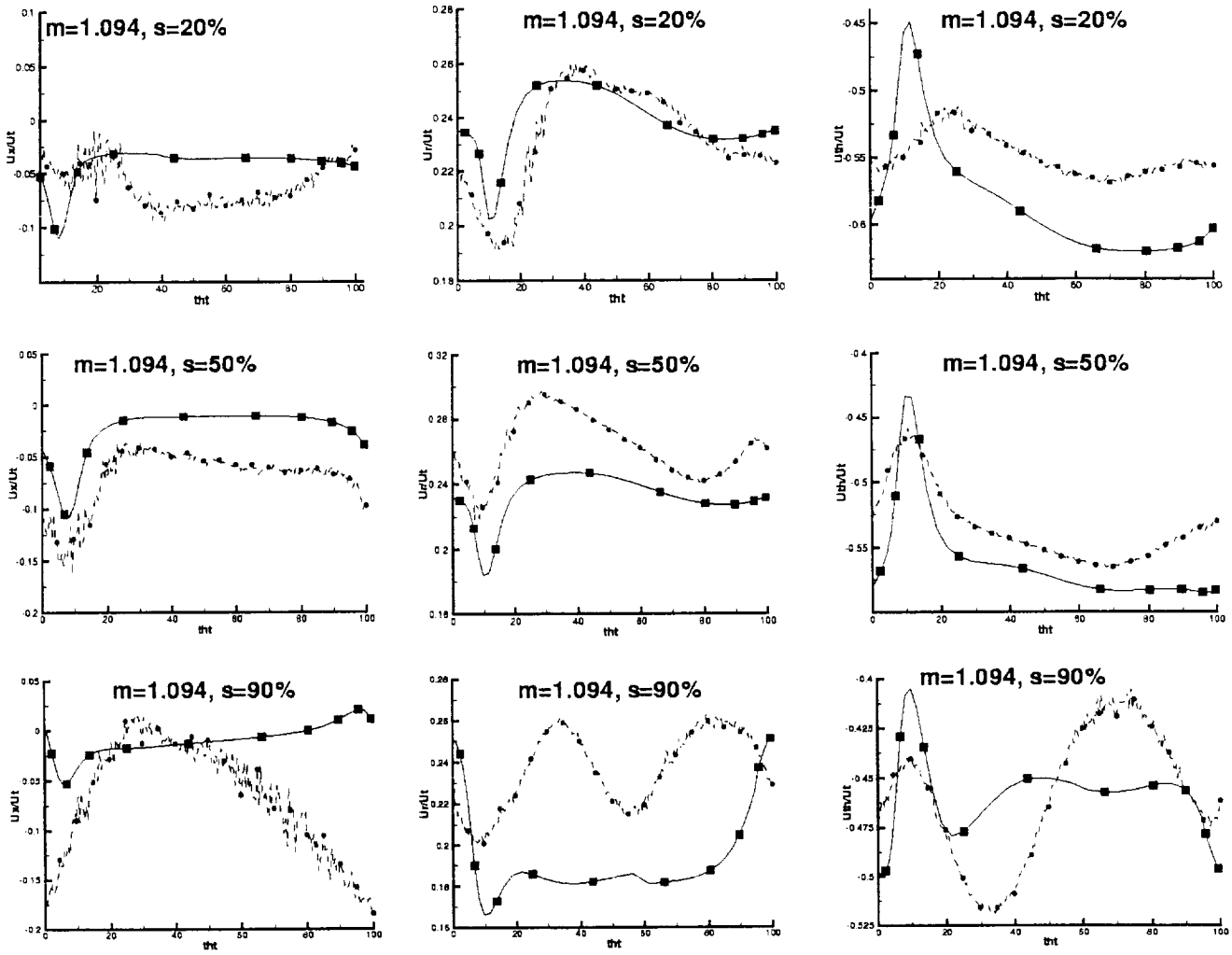

Figure 10. Comparison of axial, tangential and rotational velocity components in blade passage at 9.4 percent of chord length downstream of blade trailing edge at 20, 50 and 90 percent span stations. ---- Measured velocities, —— predicted TURBO predicted velocities.